IEEE Access
Multidisciplinary ⋮ Rapid Review ⋮ Open Access Journal

Date of publication xxxx 00, 0000, date of current version xxxx 00, 0000.

Digital Object Identifier 10.1109/ACCESS.2017.Doi Number

DFT Spread-Optical Pulse Amplitude Modulation for Visible Light Communication Systems

OSAMA SAIED[1], XINGWANG LI[2], (Member, IEEE), AND KHALED M. RABIE[3], (Member, IEEE)

[1]Computer engineering department, Biruni Remote Sensing Center (BRSC), Treq Elswany, Tripoli, Libya
[2]School of Physics and Electronic Information Engineering, Henan Polytechnic University, Jiaozuo 454000, China.
[3]Faculty of Science and Engineering, Manchester Metropolitan University, Manchester M1 5GD, U.K

Corresponding author: Osama Saied (e-mail: osama.dhawi.saied@hotmail.com).

This paragraph of the first footnote will contain support information, including sponsor and financial support acknowledgement. For example, "This work was supported in part by the U.S. Department of Commerce under Grant BS123456."

ABSTRACT DC-biased optical orthogonal frequency division multiplexing (DCO-OFDM) has been proposed in visible light communication (VLC) to overcome the limited modulation bandwidth of light emitting diode (LED). Due to the implementation of the inverse fast Fourier transform at the DCO-OFDM transmitter, DCO-OFDM suffers from its high peak-to-average power ratio (PAPR), which restricts its use in some VLC applications, especially where the optical power efficiency is a crucial requirement. That is because the LEDs used in VLC systems have a limited optical power-current linear range. To this end, a novel discrete Fourier transform spread-optical pulse amplitude modulation (DFTS-OPAM) signal scheme based on the single carrier-interleaved frequency division multiple access (SC-IFDMA) signal is introduced in this paper to address the high PAPR issue of OFDM. DFTS-OPAM is achieved by considering a PAM as an SC-IFDMA data symbol and duplicate the output vector of the fast Fourier transform at the SC-IFDMA transmitter side. Simulation results show that the PAPR of the proposed scheme is 7 dB lower than that of DCO-OFDM. Furthermore, this significant PAPR improvement is experimentally investigated where the practical results show that the proposed scheme can provide more 2.5 dB reduction in the average transmitted power requirement compared to DCO-OFDM and can subsequently increase the maximum achieved distance between the transmitter and the receiver by 44%.

INDEX TERMS single carrier frequency division multiple access, DC-biased optical orthogonal frequency division multiplexing; visible light communication, peak-to-average power ratio, light-emitting diode, dynamic range.

I. INTRODUCTION

Visible light communications (VLCs) have received a great deal of research attention as a promising candidate for future broadband networks by utilizing white light emitting diodes (LEDs) in the existing solid-state lighting (SSL) infrastructure. LEDs offer multiple usages such as illumination, high-speed data transmission and localization in various applications [1-3]. Compared to the wireless radio frequency (RF) technologies, VLC systems are energy-efficient, cost-effective, and ideal for use in hospitals, aircraft cabins or in petrochemical industries since it does not interfere with other radio frequency (RF) systems nor induces any health issues. Furthermore, VLCs occupy an unregulated portion of the electromagnetic spectrum and offer a large transmission bandwidth [1–3]. Although the wavelength of the visible light ranges from 380 to 780 nm (i.e., offers a bandwidth of up to 300 THz), the 3 dB modulation bandwidth ($3\ dB_{BW}$) of the standard high-power white phosphor LED (PWLED) that is used for illumination is only a few MHz, which limits the maximum achievable VLC data rate [1-2]. To expand the $3\ dB_{BW}$ of the LED, optical blue filtering was employed at the receiver (Rx) side to filter out the slow yellowish component of the LEDs [5]. In addition to the optical blue filtering, pre-and post-equalization methods were also proposed to extend the $3\ dB_{BW}$ of the LEDs [6-8]. For example, using pre-and post-equalizations with the emitter degenerated LED driver increase the $3\ dB_{BW}$ of the blue, red, and green LEDs by 174, 180, and 145 MHz, respectively [6]. However, these methods cause a significant reduction in the received signal-to-noise ratio (SNR) [9-10].

Alternatively, a few diversity and complex techniques have been proposed to compensate the LED modulation bandwidth

This article has been accepted for publication in a future issue of this journal, but has not been fully edited. Content may change prior to final publication. Citation information: DOI 10.1109/ACCESS.2022.3147209, IEEE Access

limitation and consequently improve the VLC data rate. Multiple input multiple output (MIMO) techniques have been studied to increase the VLC data rate. For example, higher achievable capacity results with spatial multiplexing MIMO method and higher diversity gains with repetition coding MIMO as compared to single input single output (SISO) systems are reported in [11]. The MIMO techniques have also been considered in conjunction with multi-carrier transmission in [12-13] and the link capacity has been improved with adaptive transmission in frequency selective VLC channels. In addition to MIMO techniques, multi-level modulation schemes including M-ary pulse amplitude modulation scheme has also employed in VLC to enhance its data rate as shown in [14]. PAM-single-carrier with frequency-domain equalization (PAM-SCFDE) has also been introduced in VLC systems to overcome the multipath issue and consequently increase the VLC data rates [15]. Investigating the bit and power loading features of multi carrier modulation (MCM) signals such as orthogonal frequency division multiplexing (OFDM) in VLC systems has demonstrated a significant data rate improvement. For instance, more than 15 Gbps data rates has been recently reported in [16] when the OFDM based on wavelength division multiplexing of four LEDs (i.e., RGBY) is employed.

The VLC systems uses intensity modulation and direct detection (IM/DD) where the signals are modulated to the light intensity. As a result, a bipolar and complex signal such as the traditional OFDM signal must be first converted into real and unipolar signal before modulating an LED. To make signal real and unipolar in DC-biased optical OFDM (DCO-OFDM), Hermitian Symmetry (HS) is imposed before inverse fast Fourier transform (IFFT) at a cost of halving the available electrical bandwidth [17] followed by addition of a DC-bias [18]. However, adding a DC-bias to a large peak to average power ratio (PAPR) signal, and passing it through the limited LED linear dynamic range makes this scheme unsuitable in some VLC applications where the power efficiency is a crucial requirement such as in diming control [19]. Alternatively, the IFFT properties have been again exploited to make the OFDM signal unipolar without any DC-bias requirements [20-21]. This comes at the cost of halving the spectral efficiency in comparison to the DCO-OFDM scheme which is achieved by keeping the real part of the data symbols to be blank in the pulse amplitude modulated discrete multitone (PAM-DMT) or by modulating only the odd subcarriers in asymmetrically clipped optical OFDM (ACO-OFDM). Despite their lower spectral efficiency compared to DCO-OFDM, ACO-OFDM and PAM-DMT still possess a high PAPR compared to single carrier modulation (SCM) [18]. Furthermore, the DC-bias may be needed in VLC systems to provide an illumination service and to remove the effect of the pulse shaping filter, which can convert unipolar signals to bipolar ones [18, 22].

Implementing FFT and interleaving mapping before the implementation of the IFFT at the OFDM transmitter (Tx) results in a special single carrier modulation scheme known as single carrier-interleaved frequency division multiple access (SC-IFDMA) [23-24]. Such signal has almost the same features as OFDM (i.e., bit and power loading and reduce inter-symbol interference) but a low PAPR signal such as an SCM signal [25-28]. However, the SC-IFDMA is mainly proposed as a means to improve the OFDM PAPR signal in the RF domain and has recently been modified to make it suitable for IM/DD based VLC systems [29-35].

The ACO-single carrier frequency-domain equalization (ACO-SCFDE) and the unipolar pulse amplitude modulation frequency division multiplexing (UPAM-FDM) are the two SC-IFDMA modified schemes that have recently been proposed to make the SC-IFDMA suitable for VLC systems [29-31]. To make the SC-IFDMA signal a real signal, its FFT output subcarriers at its Tx should be symmetrically conjugated. This was achieved in the U-PAM-FDM by considering a PAM as an SC-IFDMA data symbol which results in a symmetrically output FFT conjugated subcarriers excluding the first and the middle ones. To make all the U-PAM-FDM output FFT subcarriers are symmetrically conjugated, a subcarrier conjugate (SCG) block is added after the FFT implementation at the U-PAM-FDM Tx where a copy of the first and the middle subcarriers are respectively inserted after the middle and the last ones [31]. On the other hand, the output FFT subcarriers of the ACO-SCFDE are imposed to HS at the Tx to satisfy the condition for the values to be real [29-30]. However, the implementation of the HS and the SCG at the Tx of the ACO-SCFDE and the U-PAM-FDM leads to the increase in their PAPR values in comparison to the traditional SC-IFDMA [31-32].

Optical single carrier-interleaved FDM (OSC-IFDM) scheme was introduced in [33-35] to make the PAPR value of the optical SC-IFDMA as low as the PAPR value of the traditional (RF) SC-IFDMA by adopting the SC-IFDMA for VLC systems without any HS or SCG requirements. This is achieved by the time domain SC-IFDMA symbol to be repeated twice (i.e., setting the interleaving mapping factor in the frequency domain to be 2) [35]. For this, the first half of this symbol is used to transmit the real-time domain samples while the second half is used for the imaginary part. However, unlike all other modified SC-IFDMA schemes, the 1st OSC-IFDM subcarrier (DC term) had to be a modulated which is affected by the DC-bias and consequently affect all the samples in the time domain. this make SC-IFDMA scheme difficult implement in a real time [35]. Note that in VLC systems, the DC level is unmodulated as it uses for turning on the LEDs, dimming or shifting the bias levels [1-2, 19].

In this study, we propose a new discrete Fourier transform spread-optical pulse amplitude modulation (DFTS-OPAM) signaling scheme. Unlike other optical SC-IFDMA scheme, DFTS-OPAM achieve a low PAPR comparable to PAPR of the RF SC-IFDMA without compromising the system performance. In DFTS-OPAM, interleaving mapping block of the SC-IFDMA at the Tx is replaced by the repeating mapping (RM). In the RM block, the output FFT vector is repeated

This article has been accepted for publication in a future issue of this journal, but has not been fully edited. Content may change prior to final publication. Citation information: DOI 10.1109/ACCESS.2022.3147209, IEEE Access

before the IFFT block, which makes the even IFFT output samples similar to the input data symbols, and the odd output samples zeros. Therefore, making the data symbols real (i.e., PAM symbols) results in real IFFT output samples suitable for IM/DD, at the cost of halving the spectral efficiency. Since the odd samples do not carry any data in DFTS-OPAM, another DFTS-OPAM signal can be transmitted in these odd samples using the time division multiple access (TDMA) technique (i.e., providing a high data rate for multiple access services). In addition, these unused DFTS-OPAM samples can be utilized for illumination, time-domain equalization, positioning and localization. Furthermore, due to the presence of the RM block, any affected subcarrier in DFTS-OPAM can be easily compensated. The simulation results shows that the PAPR value of the DFTS-OPAM scheme is ~ 7 dB lower than the DCO-OFDM scheme. Furthermore, the effect of PAPR reduction is practically investigated, with the results showing the possible increase in the maximum achieved distance between the Tx and the Rx by up to 44% for the proposed scheme in comparison to the DCO-OFDM scheme.

The remainder of this paper is structured as follows. Section II presents the proposed DFTS-OPAM scheme. The simulation and the experimental results obtained for the proposed scheme are analyzed and discussed in Section III and Section IV, respectively. Finally, conclusions are drawn in Section V.

II. DISCRETE FOURIER TRANSFORM SPREAD OPTICAL PULSE AMPLITUDE MODULATION

In this section, the signal processing of the DFTS-OPAM scheme is illustrated and explained in detail where the reduction in the PAPR of this scheme is mathematically established and analyzed.

A. DFTS-OPAM Tx

Fig. 1 shows an example of the DFTS-OPAM Tx signal processing procedure. First, random serial binary input bits $b_i(t)$ are converted to parallel and mapped to real PAM signal i.e., $\boldsymbol{p} = \{p_0, p_1, p_2, \dots \dots \dots \dots p_{M-1}\}$, and M is the number of transmitted data symbols. The real vector $\boldsymbol{p}$ is then converted to a frequency domain by implementing the FFT operation, where the resulting FFT output sub-carriers (P) are conjugated symbols as shown in Fig. 1 and established below:

$$P_k = \sum_{m=0}^{M-1} p_m \, e^{\frac{-j2\pi mk}{M}} \tag{1}$$

$$P_{M-k} = \sum_{m=0}^{M-1} p_m \, e^{-j(\frac{2\pi m}{M})(M-k)}$$

$$= \sum_{m=0}^{M-1} p_m \, e^{-j(2\pi m - \frac{2\pi mk}{M})}$$

$$= \sum_{m=0}^{M-1} p_m \, e^{\frac{j2\pi mk}{M}} \tag{2}$$

From (1) and (2), it can be seen that each k^{th} subcarrier is conjugate of the $M - k^{th}$subcarrier (i.e., $P_k = P^*_{M-k}$), for $\boldsymbol{p}$ is a real vector. Subsequently, $\boldsymbol{P}$ is repeated twice by passed through the RM process, where the new frequency domain output symbol vector ($\boldsymbol{X}$) has a length of $N = 2M$, which is defined as:

$$\boldsymbol{X} = \{p_0, p_1, p_2, \dots p_{M-1}, p_0, p_1, p_2, \dots p_{M-1}\}$$

$$\boldsymbol{X} = \{X_0, X_1, X_2, X_3, X_4, , , , , , , , , , , , , , , \dots X_{N-1}\} \tag{3}$$

$\boldsymbol{X}$ is then converted back to the time domain samples vector ($\boldsymbol{x}$) using IFFT. However, because the IFFT operation is implemented before the RM and FFT blocks, $\boldsymbol{x}$ has as low a PAPR value as that of a SCM scheme, as shown below:

$$x_n = \frac{1}{N} \sum_{l=0}^{N-1} X_l \, e^{\frac{j2\pi ln}{N}}$$

$$x_n = \frac{1}{N} \left[\sum_{l=0}^{\frac{N}{2}-1} X_l \, e^{\frac{j2\pi ln}{N}} + \sum_{l=\frac{N}{2}}^{N-1} X_l \, e^{\frac{j2\pi ln}{N}} \right] \tag{4}$$

From (4), the following equation can be deduced:

$$x_n = \frac{1}{N} \left[\sum_{k=0}^{M-1} P_l \, e^{\frac{j2\pi nk}{N}} + \sum_{k=0}^{M-1} P_k \, e^{\frac{j2\pi n(M+k)}{N}} \right]$$

$$x_n = \frac{1}{N} \left[\sum_{k=0}^{M-1} P_l \, e^{\frac{j2\pi nk}{N}} + \sum_{k=0}^{M-1} P_k \, e^{j(\pi n + \frac{2\pi nk}{N})} \right] \tag{5}$$

Thus, the odd and even samples of $\boldsymbol{x}$ respectively defined as:

$$x_{n\_Odd} = \frac{1}{N} \left[\sum_{k=0}^{M-1} P_l \, e^{\frac{j2\pi nk}{N}} - \sum_{k=0}^{M-1} P_l \, e^{\frac{j2\pi nk}{N}} \right] = 0 \tag{6}$$

$$x_{n\_Even} = \frac{1}{2M} \left[\sum_{k=0}^{M-1} P_l \, e^{\frac{j2\pi nk}{M}} + \sum_{k=0}^{M-1} P_l \, e^{\frac{j2\pi nk}{M}} \right] \tag{7}$$

$$x_{n\_Even} = \frac{1}{M} \sum_{k=0}^{M-1} P_l \, e^{\frac{j2\pi nk}{M}}$$

From (6) and (7), one can see that x_{n_Even} is a repeated signal of p_m, while no samples are carried on x_{n_Odd} (i.e., $x_{n\_Odd} = 0$ (see Fig. 1)). Note that, as DFTS-OPAM uses PAM as a modulation technique, its spectral efficiency is a half of that of the DCO-OFDM scheme (i.e., has the same spectral efficiency as ACO-OFDM). Furthermore, because of the RM process, any distorted subcarrier in this scheme can be easily recovered. Finally, $\boldsymbol{x}$ is passed through the parallel to serial (P/S) converter, cyclic prefix (CP) insertion, digital analogue converter (DAC), low pass filter (LPF), DC-bias, clipping, and electrical to optical converter (EOC) blocks.

This article has been accepted for publication in a future issue of this journal, but has not been fully edited. Content may change prior to final publication. Citation information: DOI 10.1109/ACCESS.2022.3147209, IEEE Access

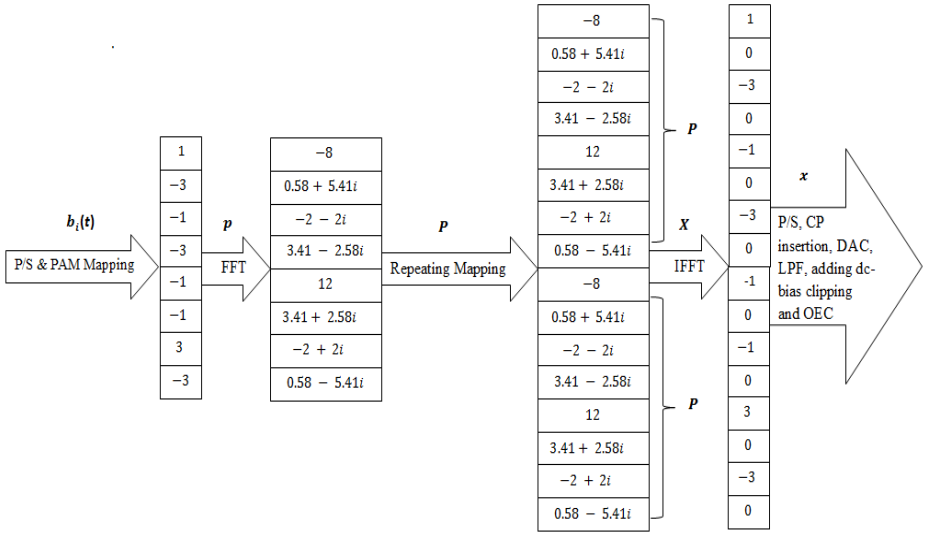

FIGURE 1. **An example of the DFTS-OPAM Tx signal processing procedure.**

B. DFTS-OPAM Rx

Fig. 2 depicts the block diagram of the DFTS-OPAM Rx. Firstly, the transmitted optical signal is converted to an electrical signal by the photodetector (PD). Furthermore, to account for shot noise due to the photocurrent fluctuations and thermal noise due to the receiver electronics, additive white Gaussian noise (AWGN) is added to the electrical signal. Hence, the resulting analogue electrical signal $r(t)$ is given by $r(t) = s(t) * h(t) + n(t)$, where $s(t)$ is the transmitted electrical signal, $h(t)$ is the time domain system impulse response, $n(t)$ is the AWGN, and the symbol * denotes the linear convolution operation (note that the PD is considered to be ideal (i.e., PD responsivity = 1)). $r(t)$ is then passed through the LPF, analogue digital converter (ADC), CP removal, and serial to parallel (S/P) blocks, where the resulting digital signal $d(t)$ of the aforementioned processes is converted to the frequency domain $Y(F)$ by FFT operation. Note that, since CP converts the linear convolution induced by the system to circular convolution (i.e., multiplication in the frequency domain), $Y(F)$ is given by:

$$Y(F) = X(F)H(F) + N(F) \tag{8}$$

where, $H(F)$ is the transfer function of the system. The transmitted signals are subsequently estimated by implementing the zero-forcing (ZF) equalizer, i.e.

$$\check{X}(F) = \frac{Y(F)}{\hat{H}(F)} \tag{9}$$

where, $\hat{H}(F)$is the estimated transfer function of the system. If the full knowledge of the channel state is known (i.e., $\hat{H}(F) \approx H(F)$, then

$$\check{X}(F)=X(F) \tag{10}$$

After that, the redundant subcarriers, including the DC subcarrier and repeated subcarriers, are removed by passing $\check{X}(F)$ through the redundancy removal process. However, because of the RM process at Tx (i.e., $\check{X}(F) = [\check{X}(F)/2\ \check{X}(F)/2]$ (see shown in Fig.1)), removing these redundant subcarriers does not cause any loss of information after compensating the first subcarrier by the middle one. Finally, the resulting signal from the redundancy removal process ($\hat{P}(F)$) is converted back to the time domain by implementing an IFFT where the output IFFT vector ($\hat{p}(t)$) passing through the PAM de-mapping and hard decision processes, to reconstruct the transmitted bits sequence.

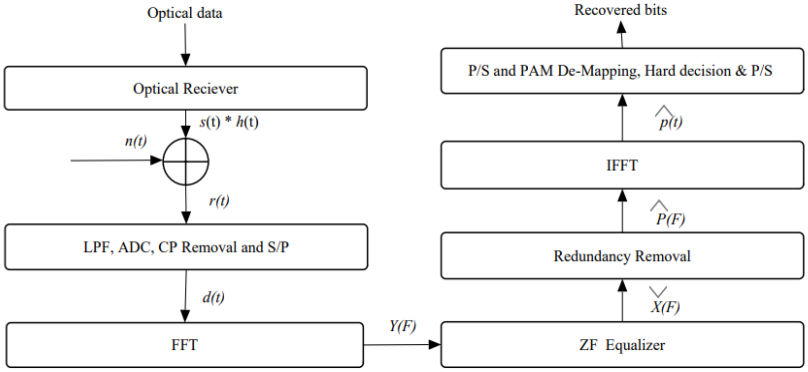

FIGURE 2. **Block diagram of the DFTS-OPAM Rx.**

This article has been accepted for publication in a future issue of this journal, but has not been fully edited. Content may change prior to final publication. Citation information: DOI 10.1109/ACCESS.2022.3147209, IEEE Access

III. SIMULATION RESULTS

The reduction of the PAPR value of OFDM in IM/DD systems was mathematically established in the previous section by implementing the FFT and RM processes before the implementation of the IFFT method. In this section, the simulation results are presented to establish the PAPR reduction using the DFTS-OPAM scheme compared to DCO-OFDM.

To obtain fair comparison between DFTS-OPAM and DCO-OFDM in terms of the SNR, bit error rate (BER), and error vector magnitude (EVM) in this section, as well as in the next section, the PAM symbols of DFTS-OPAM are generated by separating the real and the imaginary parts of quadrature amplitude modulation (QAM) symbols [i.e., QAM symbol $(a + ib)$ is separated into 'a' and 'b' PAM symbols], where these symbols are combined at the Rx to reconstruct the QAM. In this simulation study, 256 IFFT points, 16-QAM constellation, 1W white LED with PCB (HPB849KxWDx) that has 1 V linear range, Thorlabs (PDA36A-EC) PD [36], AWGN channel and 2 µsc CP duration are considered.

The PAPR values of the discrete signal is given by:

$$PAPR = \frac{\max\ |x_n|^2;\quad n = 0, \dots N-1}{\mathrm{E}\{|x_n|^2\}} \qquad (12)$$

where $x_n, \max |x_n|^2$ and $\mathrm{E}\{|x_n|^2\}$ are the discrete-time signal, the peak power of x_n, and the average power of x_n, respectively.

To compare the PAPRs, the complementary cumulative distribution function (CCDF) of both schemes is simulated and given in Fig. 3 whereas all the PAPR comparisons are carried out at CCDF= 10^{-4} (i.e.,$\Pr\{\mathrm{PAPR} > \mathrm{PAPR}_0\} = 0.0001$) as in other work (e.g., in [37-38]). Fig. 3 plots the CCDF again the PAPRs of the DFTS-OPAM and DCO-OFDM schemes. The figure demonstrates that the PAPR of the proposed scheme is ~ 7 dB lower than the PAPR value of the DCO-OFDM scheme.

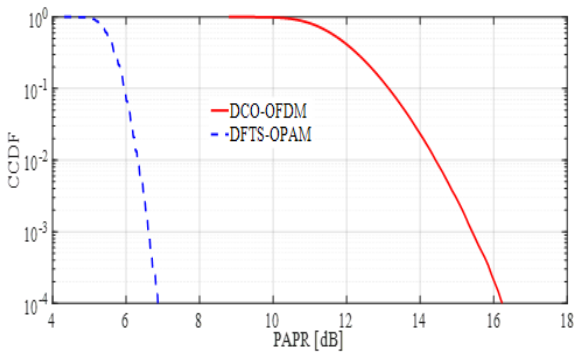

FIGURE 3. CCDF versus PAPR of the DCO-OFDM and DFTS-OPAM schemes.

Fig.4 depicts the BER performance against the SNR (dB) for the DCO-OFDM and DFTS-OPAM schemes for 16-QAM. The figure shows that DCO-OFDM requires ~ 3 dB more SNR in comparison to DFTS-OPAM to achieve the BER value of 10^{-6}. This is because, only the even time-domain samples carry data in DFTS-OPAM, while all the samples are used to carry data in DCO-OFDM, making the DCO-OFDM scheme have double the spectral efficiency of DFTS-OPAM.

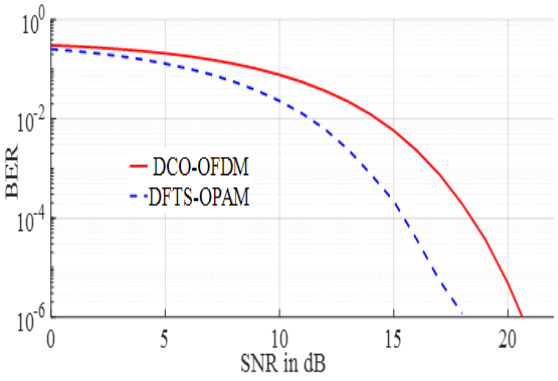

FIGURE 4. SNR versus BER for 16-QAM DCO-OFDM and 16-QAM DFTS-OPAM.

In VLC systems, the average transmitted power (P_{avg}) of the OFDM scheme is limited by the dynamic range of the LED where any signal above the LED limited linear range will be distorted or clipped, which affects the VLC system performance, since a lower P_{avg} leads to a lower SNR (i.e., leads to a shorter distance between the Tx and the Rx and/or lower constellation mapping order). Figs. 5-7 depict the maximum transmitted average power (P_{max}) that can be achieved by the two schemes. Note that P_{avg} of both schemes was varied from 0 dBm to 25 dBm in the simulations, and the EVM was simulated at each P_{avg} value, where P_{max} is predicted to occur for EVM=12.5%, as the system performance begins to deteriorate after this EVM% value [39-40].

Figs. 5 and 6 illustrate the 16-QAM constellation points of the DCO-OFDM and the DFTS-OPAM schemes, respectively for EVM = 12.5%, where only the clipping noise was considered (i.e., no AWGN) in the simulations, and the DC-bias of both schemes was set to be at the center point of the LED dynamic range (note that, the dynamic range of the LED in these simulations was 1 V). In these figures, P_{max} of the DCO-OFDM and DFTS-OPAM schemes are 17.42 dBm and 19.32 dBm, respectively (i.e., DFTS-OPAM provides approximately 2 dBm more P_{avg} in comparison to DCO-OFDM, when only the clipping noise is considered). Furthermore, Fig. 6 shows that the clipping noise in DFTS-OPAM is a linear noise.

Since the AWGN power (P_{awgn}) (i.e., the noise power of the VLC system) increases the EVM, P_{max} will be affected by the amount of P_{awgn} present in the system. Note in [30-31], the P_{awgn} was set to -10 dBm. However, the noise power in VLC systems varies within a range as it depends on numerous parameters [1-3]. In Fig. 7, the P_{awgn} is varied from -15 dBm to 0 dBm, and P_{avg} of both schemes is evaluated at each P_{awgn} value to identify P_{max}, which as previously mentioned,

This article has been accepted for publication in a future issue of this journal, but has not been fully edited. Content may change prior to final publication. Citation information: DOI 10.1109/ACCESS.2022.3147209, IEEE Access

is achieved when EVM = 12.5%. From this figure, one can observe that increasing P_{awgn} decreases the P_{max} value of both schemes, as the EVM becomes more sensitive to the clipping noise by increasing the P_{awgn} level. An additional observation made from the figure is that for a 1 V LED dynamic range, the 16-QAM DCO-OFDM signaling scheme can only be implemented when the $P_{awgn} \leq$ -7 dBm, as greater P_{awgn} values result in increasing the EVM beyond the 12.5% level. However, 16-QAM-DFTS-OPAM can tolerate higher noise power levels, as it can be implemented using the same given parameters for $P_{awgn} \leq$ -1 dBm. Furthermore, the figure also demonstrates that the 16-QAM DFTS-OPAM scheme outperforms the 16-QAM-DCO-OFDM scheme for all noise power levels in terms of transmit power efficiency.

Finally, since LEDs are mainly used for illumination purposes, controlling the brightness of LEDs should be taken into consideration in VLC systems. One straightforward method used to control the brightness of LEDs is to adjust the DC-bias level [19, 41-42]. However, increasing or decreasing the DC-bias level results in increasing the upper or lower clipping noise of the bipolar OFDM schemes respectively. Note that, in Fig. 7, the DC-bias was set to be at the middle point of the LED linear range, thus providing a fixed illumination level. However, to study the effect of the brightness control on the system performance of 16-QAM DFTS-OPAM and 16-QAM DCO-OFDM, the DC-bias level was set at the first and third quarter points of the LED linear range, thus providing three diming control levels. The effect of setting the DC-bias at the first and third quarter points of the LED dynamic range on the system performance of the two schemes is illustrated in Figs 8 and 9, respectively.

However, as both schemes are bipolar OFDM schemes, in Fig. 8, the system performance of both schemes is mostly affected by the lower clipping noise, while in Fig. 9, the upper clipping noise is the dominant clipping noise for both schemes. Furthermore, setting the DC-bias at the first quarter point of the LED linear range provides the same performance as setting it at the third quarter-point. This is because both schemes have a normal Gaussian distribution shape (i.e., the lower clipping noise in Fig.8 is the same as the upper clipping noise in Fig. 9). In addition, from these figures, it can observe that setting the DC-bias at these two points of the LED linear range makes the DCO-OFDM and DFTS-OPAM schemes only valid (i.e., EVM > 12.5%) for $P_{awgn} \leq$ -12 dBm and $\leq$ -7 dBm, respectively.

Furthermore, increasing of the P_{awgn} level results in decreasing P_{max} from 13.4 dBm to 12.8 dBm, and from 12 dBm to 10.3 dBm, for 16-QAM DFTS-OPAM and 16-QAM DCO-OFDM, respectively. Note that diming control can also be achieved in VLC systems by controlling the pulse samples duration [42]. However, since the odd samples in DFTS-OPAM do not carry any data, the duration of the even samples of this scheme have more flexibility to be adjusted according to the required illumination level, as will be demonstrated in our future work.

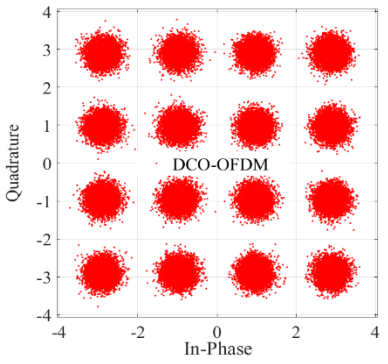

FIGURE 3. ***The 16-QAM constellation points of DCO-OFDM, where $P_{max} = 17.42$ dBm, EVM%=12.5%, LED dynamic range = 1V, and only the clipping noise is considered (i.e., no AWGN).***

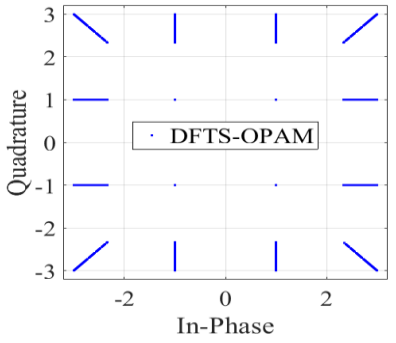

FIGURE 4. ***The 16-QAM constellation points of DFTS-OPAM, where $P_{max} = 19.32$, EVM%=12.5%, LED dynamic range = 1V, and only the clipping noise is considered (i.e., no AWGN).***

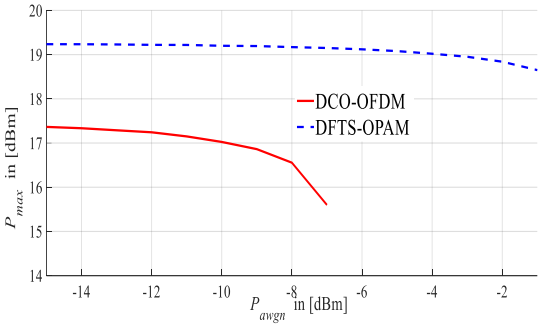

FIGURE 5. ***P_{max}*** **with respect to** ***P_{awgn}*** **of the DCO-OFDM and B-PAM-FDM schemes, when the DC-bias is set in the middle of the LED dynamic range.**

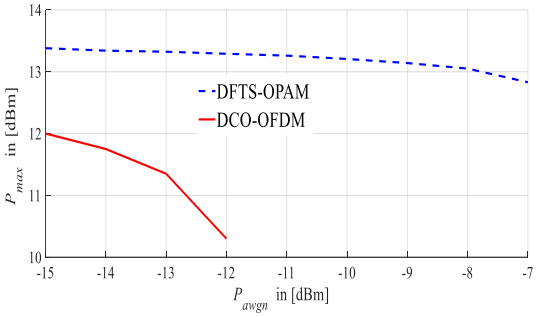

FIGURE 6. ***P_{max}*** **with respect to** ***P_{awgn}*** **of the DCO-OFDM and B-PAM-FDM schemes, when DC-bias is set at the first quarter of the LED dynamic range**

This article has been accepted for publication in a future issue of this journal, but has not been fully edited. Content may change prior to final publication. Citation information: DOI 10.1109/ACCESS.2022.3147209, IEEE Access

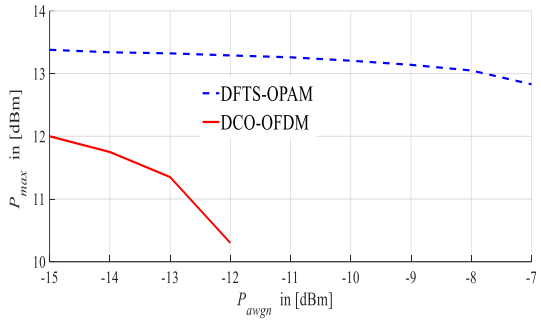

FIGURE 7. P_{max} **with respect to** P_{awgn} **of the DCO-OFDM and B-PAM-FDM schemes, when DC-bias is set at the third quarter of the LED dynamic range.**

IV. EXPERIMENTAL RESULTS

The main aim of this experimental study was to implement the DFTS-OPAM signaling scheme in real time using the USRP N210 transceiver, and practically support the illustrated theory of the proposed DFTS-OPAM by practically proving low PAPR compared to DCO-OFDM in terms of providing more P_{max}, and thus increasing the distance between the Tx and Rx (de). The P_{avg} of the aforementioned two schemes are varied from 0 dBm to 24 dBm at the Tx side where the effect of this variations on the system performance was verified at the Rx.

Figs. 10 and 11 illustrate the experimental setup configuration and the setup hardware, respectively.

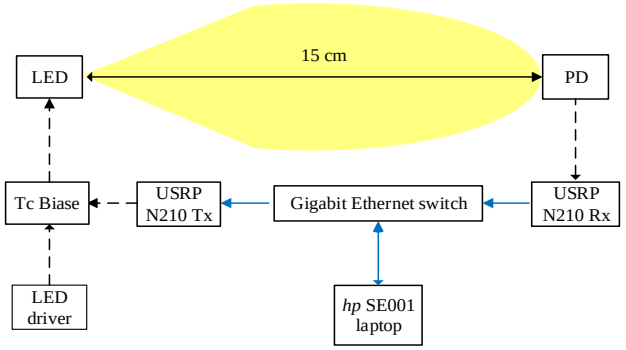

FIGURE 8. **Experimental setup diagram.**

FIGURE 9. **A photograph of the experimental hardware.**

The USRP transceiver was interfaced and controlled by a laptop through LabVIEW software where the main Tx and Rx parameters used are presented in Figs. 12 and 13.

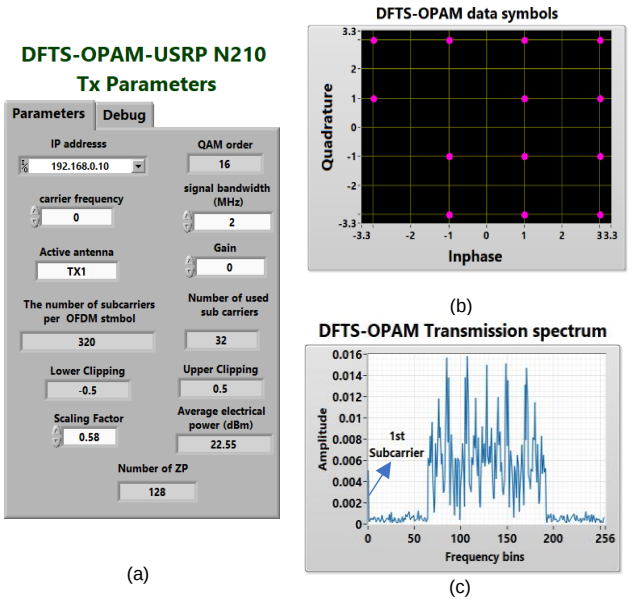

FIGURE 10. **LabVIEW control panel of the USRP Tx of DFTS-OPAM, where plots (a), (b) and (c) depict the DFTS-OPAM Tx parameters, the DFTS-OPAM transmitted QAM symbols, and the DFTS-OPAM transmitted spectrum, respectively.**

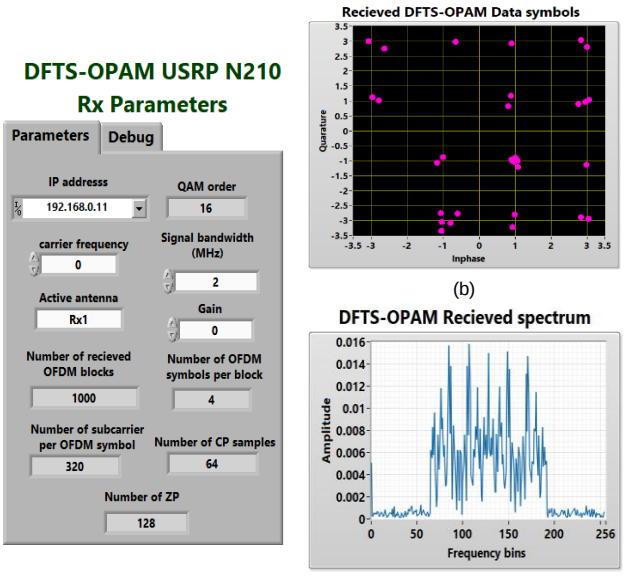

FIGURE 11. **LabVIEW control panel of the USRP Rx of DFTS-OPAM. Note that the 16-QAM constellation points in (b) were captured at EVM = 10.2%).**

At the Tx, 640 and 1280 bits were randomly generated, separately mapped to 16-QAM, saved and used to implement one DFTS-OPAM block and one DCO-OFDM block respectively (i.e., 160 and 320 complex QAM data symbols for each DFTS-OPAM block and each DCO-OFDM block,

This article has been accepted for publication in a future issue of this journal, but has not been fully edited. Content may change prior to final publication. Citation information: DOI 10.1109/ACCESS.2022.3147209, IEEE Access

respectively) where each block consists of 5 different -time domain OFDM symbols (i.e., 32 and 64-QAM data symbols used for each DFTS-OPAM time domain -symbol and DCO-OFDM time domain symbol, respectively). Note that, for DFTS-OPAM scheme, the imaginary and the real parts of the QAM data symbols were separated to provide 64 PAM symbols before applying the FFT process. As in LTE [43], to practically remove the inter-channel interference (ICI) issue, the DFTS-OPAM and the DCO-OFDM schemes were zero-padded (i.e., adding zeros at the edge of the subcarriers, before being passed to the IFFT process). As illustrated in Fig. 14, because of this process (i.e., zero-padding process) the DFTS-OPAM subcarriers are not conjugated subcarriers anymore. This result in the output IFFT samples of DFTS-OPAM complex samples. To make all DFTS-OPAM subcarriers are conjugated after the zero padding a few modifications is been done as illustrated in Fig 15.

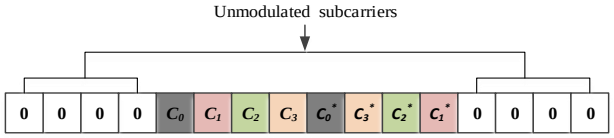

FIGURE 12. DFTS-OPAM subcarriers after inserting 8 zeros at both edges (note that in this figure, the number of subcarriers before ZP is 8).

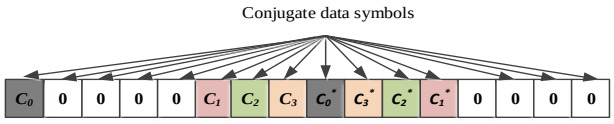

FIGURE 13. The DFTS-OPAM subcarriers after shifting the first subcarrier to the beginning.

A 1 W white LED (HPB8-49KxWDx) introduced in the simulation section was used in this experiment where its measured L-I-V curve is shown in Fig. 16. To ensure operation in the linear region, the LED was biased at the middle point of its dynamic range (i.e., at 500 mA), providing 1 V peak to peak voltage.

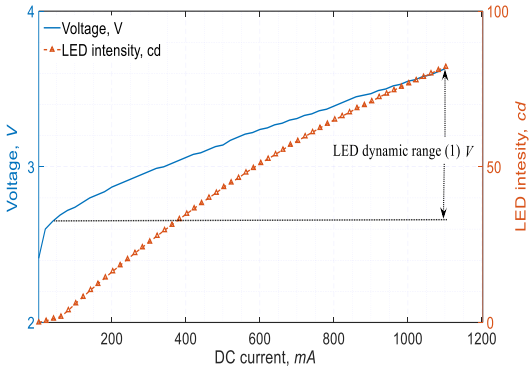

FIGURE 14. Measured L-I-V curves of the 1 W white LED (HPB8-49KxWDx).

At the Rx, the light signal was detected and converted back to an electrical signal by the (PDA36A-EC) PD, which is first captured by USRP Rx, then transfer to the laptop for application of signal processing and analysis (see Figs.10 and 11). 1000 OFDM blocks for each scheme were received and processed online where each block had 5 different OFDM time domain symbols and the average result was considered. The maximum likelihood (ML) algorithm was applied in this experimental work to each OFDM block for synchronization and frequency offset correction purposes, by investigating the length of the CP samples [44] (64 samples were used as CP in this work), as shown in Fig. 17.

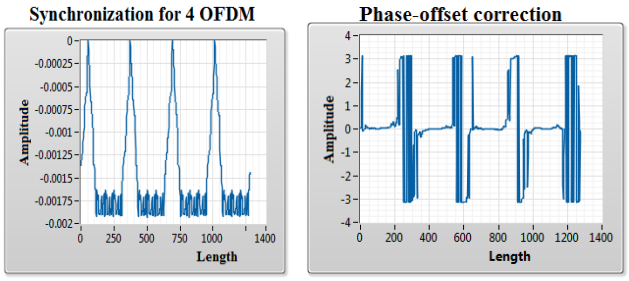

(a) (b)

FIGURE 15. ML algorithm applied to an OFDM block to achieve: (a) synchronization estimation, and (b) frequency offset estimation.

Following the implementation of the ML algorithm, each OFDM time domain symbol was fed to the FFT process, where the redundant output subcarriers (i.e., the zero-padded and conjugate subcarriers for the DCO-OFDM scheme and the ZP and repeated subcarriers for DFTS-OPAM scheme) were rejected. Note that, because of the RM process, the first DFTS-OPAM subcarrier affected by DC-bias was replaced by the middle subcarrier in this work. Since the transmitted bits were randomly generated, saved and repeatedly transmitted, 8 subcarriers from each OFDM time domain symbol were used as the data and the pilots were investigated to estimate the transfer function of the system [3]. After estimating the transfer function of the system, the ZF algorithm was implemented to equalize the OFDM data symbols. Finally, the transmitted bits of DCO-OFDM and DFTS-OPAM were reconstructed from the equalized data symbols and saved to be processed offline by a MATLAB program for BER and EVM assessment. P_{max} of the DCO-OFDM and DFTS-OPAM schemes was experimentally evaluated by measuring the EVM at each P_{avg} value within the range $0 \leq P_{avg} \leq 24$ (note that, $P_{max} = P_{avg}$ when EVM = 12.5%). Furthermore, the benefit of the P_{max} the penalty was investigated by increasing the distance between the Tx and the Rx.

Fig. 18 plots the EVM versus P_{avg} of the 16-QAM DCO-OFDM and 16-QAM DFTS-OPAM schemes for *de* = 15 cm. The figure shows that for $P_{avg} \leq 18$ dBm, the EVM of both schemes decreased by increasing P_{avg}, since the SNR is increased. However, for $P_{avg} > 18$ dBm, the EVM of DCO-OFDM started increasing and the system performance started to deteriorate, as the linear range of the system was no longer

This article has been accepted for publication in a future issue of this journal, but has not been fully edited. Content may change prior to final publication. Citation information: DOI 10.1109/ACCESS.2022.3147209, IEEE Access

applicable at this value. On the other hand, the system performance of DFTS-OPAM started to deteriorate by the clipping noise when P_{avg} > 22 dBm. The figure also demonstrates that the measured P_{max} of the DCO-OFDM and DFTS-OPAM was 20.5 dBm and 22.5 dBm, respectively (i.e., the DFTS-OPAM provided 2 dB more P_{avg} in comparison to DCO-OFDM). Furthermore, for P_{avg} < 18 dBm, DCO-OFDM required around 3 dB more SNR in comparison to DFTS-OPAM to achieve the same EVM % levels, since the odd samples do not carry any data in the DFTS-OPAM scheme (see Fig. 3 in the simulation results).

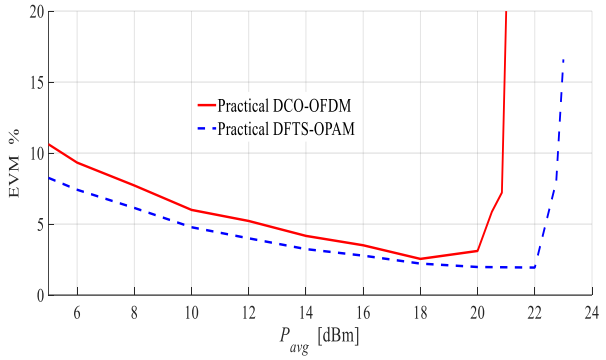

FIGURE 16. The EVM% with respect to P_{avg} for 16 QAM DCO-OFDM and 16 QAM B-PAM-FDM.

Following the previous discussions, higher P_{avg} values result in increasing the distance between the Tx and Rx. To determine the maximum achievable distance between the Tx and the Rx (d_{max}) for both schemes, P_{avg} of both schemes is set at P_{max}, *de* is increased progressively, and the EVM is measured at each *de* value, where d_{max} is achieved when EVM = 12.5% (Note that P_{max} in Fig 18 occurs for *de* = 15 cm). However, as already discussed in the simulation results (see Fig. 7), decreasing the SNR value (i.e., increasing *de)* reduces P_{max}. As such, for *de* > 15 cm, a lower P_{max} should be used (i.e., lower than 20.5 dBm and 22.5 dBm for DCO-OFDM and DFTS-OPAM respectively). In this investigation, P_{avg} values of 20.25 dBm and 22.25 dBm, which occurred in Fig 18 for *de* = 15 cm when EVM = 7.5%, were considered as the optimum average power (P_{opt}) levels for the DCO-OFDM and DFTS-OPAM schemes respectively, as they can be used for a range of SNR values (i.e., for a range of distances).

In Fig. 19, P_{avg} of each scheme was set to its P_{opt}, *de* was varied within the range 15 cm ≤ *de* ≤ 70 cm, and the EVM was measured after each 2 cm. From this figure, it can be seen that the EVM of DCO-OFDM and DFTS-OPAM reach the threshold value (i.e., EVM = 12.5%) for *de* = 43 cm and 63 *cm*, respectively. As such, implementing the proposed scheme increased *de* by up to 44% in comparison to the traditional DCO-OFDM scheme. Note that, in Fig 19, to ensure that the achieved distance is the maximum one for both schemes, P_{avg} of both schemes was kept around their P_{opt}values, and $d_{max}$was achieved when P_{avg}=P_{opt}.

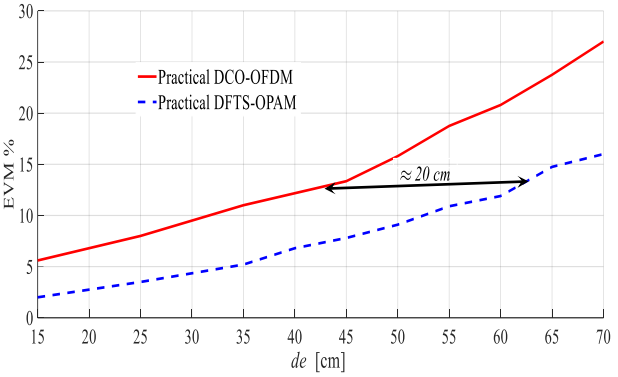

FIGURE 17. EVM% versus *de* for the 16-QAM DCO-OFDM and 16 QAM B-PAM-FDM schemes, where P_{avg} of DCO-OFDM and B-PAM-FDM is 20.25 dBm and 22.25 dBm, respectively.

Finally, the BER performance of the two schemes was investigated experimentally as a function of *de*, as illustrated in Fig. 20, where P_{avg} of both schemes was set at their P_{opt}. The figure demonstrates that for *de* < 45 cm, both schemes achieved the same BER performance (i.e., both schemes reached the noise floor), as the EVM of the two schemes was less than 12.5% for shorter distances. However, for *de* ≥ 45 cm, the BER performance of DCO-OFDM is being affected as its SNR is dropped down and consequently, the EVM become more than 12.5% while the BER performance of the DFTS-OPAM scheme is start being affected when *de* > 65 cm, which is because the P_{avg} of the proposed scheme is around 2 dBm more than the $P_{avg}$of the traditional DCO-OFDM.

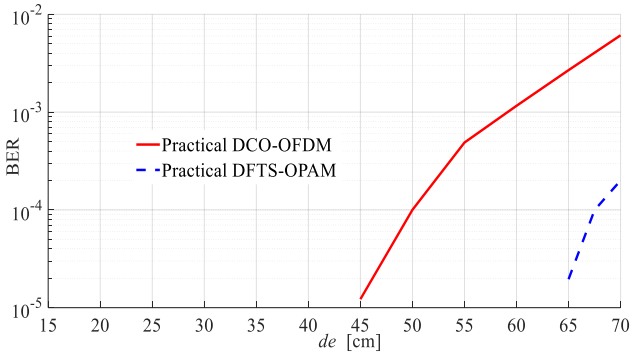

FIGURE 18. The BER with respect to *de* for both 16-QAM DCO-OFDM and 16-QAM B-PAM-FDM where, P_{avg} of DCO-OFDM and B-PAM-FDM are 20.25 dBm and 22.25 dBm respectively.

However, in a real scenario, the VLC link distance between the Tx and the Rx should be > 150 cm [1-2, 19]. In fact, VLC link distance depends on several parameters such as: transmitted average power, divergence angle at the Tx, Rx field of view (FOV), Rx sensitivity, measuring devices, amplifier at the Rx, optical filter, Rx non-imaging concentrator internal reflective index, modulation depth, and data rate etc [2, 45]. Note, because of the limited optical wireless communication Lab equipment that we have and because the main reason behind this work is to introduce the new novel DFTS-OPAM scheme first time and compare it with the

This article has been accepted for publication in a future issue of this journal, but has not been fully edited. Content may change prior to final publication. Citation information: DOI 10.1109/ACCESS.2022.3147209, IEEE Access

known DCO-OFDM scheme in term of their PAPR for the same given parameters, we have by MATLAB simulation proven that changing few parameters (i.e., LED semi angle at half-power (θ1/2), QAM order and Non-imaging concentrator internal reflective index) on our practical experiment can increase the maximum achievable distance between the Tx and the Rx to be more than 150 cm as illustrated in Figures 21, 22 and 23 at the Appendix Section where the VLC simulation parameters that were used for these plots are also illustrated at the same Section in Table 1.

VII. CONCLUSION

The proposed DFTS-OPAM were introduced in this paper as means to significantly improve the PAPR of the OFDM signal in IM/DD based VLC systems, by making SC-IFDMA scheme suitable for IM/DD without any HS requirements. This IM/DD compatibility is achieved in DFTS-OPAM by replacing the interleaving mapping block in the SC-IFDMA Tx by the RM block and using PAM as a modulation scheme. As such, the output time domain samples of the IFFT are bipolar real samples that have as low PAPR as that of the SCM scheme.

The simulation results of DFTS-OPAM showed that the PAPR value of DFTS-OPAM is 7 dB lower than the PAPR value of the traditional DCO-OFDM scheme. The results also showed that the DCO-OFDM requires 3 dB more SNR in comparison to DFTS-OPAM to achieve the same BER performance. The impact of this PAPR reduction on the system performance was experimentally investigated, where the results showed that the maximum achieved distance between the Tx and Rx was increased by up to 44% when the DFTS-OPAM scheme was implemented compared to DCO-OFDM.

APPENDIX

TABLE I
VLC SIMULATION PARAMETERS

Parameters	Value
Number of iterations	10^6
LED Type	1W white LED with PCB (HPB849KxWDx)
LED bandwidth	2MHz
LED linearity	~1 V
Photodetector (PD)	Thorlab (PDA36A-EC)
PD bandwidth	10 MHz
PD noise (RMS)	300 μV
PD responsivity	0.65 A/W
PD active area	16 mm^2
Rx FOV	20^0

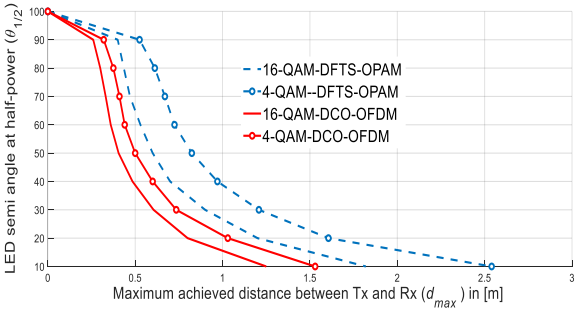

FIGURE 19. d_{max} versus $\theta_{1/2}$ for 16 QAM B-PAM-FDM, 4 QAM-BPAM-FDM, 16 QAM DCO-OFDM and 4 QAM-DCO-OFDM

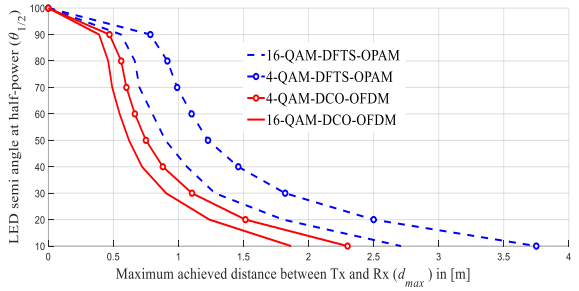

FIGURE 20. d_{max} versus $\theta_{1/2}$ for 16 QAM B-PAM-FDM, 4 QAM-BPAM-FDM, 16 QAM DCO-OFDM and 4 QAM-DCO-OFDM when *1.5* Non-imaging concentrator internal reflective index is used at the Rx.

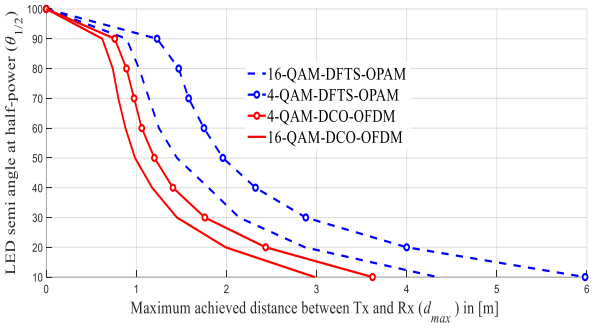

FIGURE 21. d_{max} versus $\theta_{1/2}$ for 16 QAM B-PAM-FDM, 4 QAM-BPAM-FDM, 16 QAM DCO-OFDM and 4 QAM-DCO-OFDM when *2.4* Non-imaging concentrator internal reflective index is used at the Rx.

REFERENCES

[1] P. A. Hoeher, Visible Light Communications: Theoretical and Practical Foundations. Munich, Germany: Hanser Fachbuch, 2019.

[2] Z. Ghassemlooy, L. N. Alves, S. Zvanovec, and M. Khalighi, *Visible Light Communications: Theory and Applications*. Boca Raton: CRC Press, 2017.

[3] O. Saied, "Orthogonal Frequency Division Multiplexing for Indoor Visible Light Communication Links," Ph.D. dissertation. Northumbria University, Newcastle Upon Tyne, UK, 2018.

[4] M. Uysal, F. Miramirkhani, O. Narmanlioglu, T. Baykas and E. Panayirci, "IEEE 802.15.7r1 Reference Channel Models for Visible Light Communications," *IEEE Communications Magazine*, vol. 55, no. 1, pp. 212-217, Jan. 2017, doi: 10.1109/MCOM.2017.1600872CM.

[5] S. Wang *et al.*, "A high-performance blue filter for a white-led-based visible light communication system," *IEEE Wireless Communications*, vol. 22, no. 2, pp. 61-67, Apr. 2015, doi: 10.1109/MWC.2015.7096286.

[6] N. Fujimoto and S. Yamamoto, "The fastest visible light transmissions of 662 Mb/s by a blue LED, 600 Mb/s by a red LED, and 520 Mb/s by

a green LED based on simple OOK-NRZ modulation of a commercially available RGB-type white LED using pre-emphasis and post-equalizing techniques," in *The European Conference on Optical Communication (ECOC)*, Cannes, France, 2014, pp. 1-3, doi: 10.1109/ECOC.2014.6963895.

[7] X. Huang, Z. Wang, J. Shi, Y. Wang and N. Chi, "1.6 Gbit/s phosphorescent white LED based VLC transmission using a cascaded pre-equalization circuit and a differential outputs PIN receiver", *Opt. Express*, vol. 23, no. 17, pp. 22 034-22 042, Aug. 2015, doi.org/10.1364/OE.23.022034.

[8] H. Li, X. Chen, J. Guo and H. Chen, "A 550 Mbit/s real-time visible light communication system based on phosphorescent white light LED for practical high-speed low-complexity application", *Opt. Express*, vol. 22, no. 22, pp. 27203-27213, Nov. 2014, doi.org/10.1364/OE.22.027203.

[9] P. A. Haigh, Z. Ghassemlooy, S. Rajbhandari, I. Papakonstantinou and W. Popoola, "Visible Light Communications: 170 Mb/s Using an Artificial Neural Network Equalizer in a Low Bandwidth White Light Configuration," *Journal of Lightwave Technology*, vol. 32, no. 9, pp. 1807-1813, May. 2014, doi: 10.1109/JLT.2014.2314635.

[10] X. Li, Z. Ghassemlooy, S. Zvanovec, R. Perez-Jimenez and P. A. Haigh, "Should Analogue Pre-Equalisers be Avoided in VLC Systems?," *IEEE Photonics Journal*, vol. 12, no. 2, pp. 1-14, Apr. 2020, doi:10.1109/JPHOT.2020.2966875.

[11] T. Fath and H. Haas, "Performance Comparison of MIMO Techniques for Optical Wireless Communications in Indoor Environments," *IEEE Transactions on Communications*, vol. 61, no. 2, pp. 733-742, Feb. 2013, doi:10.1109/TCOMM.2012.120512.110578.

[12] Y. Hong, T. Wu and L. Chen, "On the Performance of Adaptive MIMO-OFDM Indoor Visible Light Communications," *IEEE Photonics Technology Letters*, vol. 28, no. 8, pp. 907-910, Apr. 2016, doi: 10.1109/LPT.2016.2517192.

[13] O. Narmanlioglu, R. C. Kizilirmak, T. Baykas and M. Uysal, "Link Adaptation for MIMO OFDM Visible Light Communication Systems," *IEEE Access*, vol. 5, pp. 26006-26014, Nov. 2017, doi: 10.1109/ACCESS.2017.2771333.

[14] M. Wolf and M. Haardt, "On the DC balance of multi-level PAM VLC systems," *in 21st International Conference on Transparent Optical Networks (ICTON)*, Angers, France, 2019, pp. 1-5, doi: 10.1109/ICTON.2019.8840531.

[15] A. Nuwanpriya, S. Ho, J. A. Zhang, A. J. Grant and L. Luo, "PAM-SCFDE for Optical Wireless Communications," *Journal of Lightwave Technology*, vol. 33, no. 14, pp. 2938-2949, 2015, doi: 10.1109/JLT.2015.2424456.

[16] R. Bian, I. Tavakkolnia and H. Haas, "15.73 Gb/s Visible Light Communication with Off-the-Shelf LEDs," *Journal of Lightwave Technology*, vol. 37, no. 10, pp. 2418-2424, May. 2019, doi: 10.1109/JLT.2019.2906464.

[17] O. Saied, Z. Ghassemlooy, X. Tang, X. Dai, H. Le Minh and B. Lin, "Position Encoded Asymmetrically Clipped Optical Orthogonal Frequency Division Multiplexing in Visible Light Communications," *Journal of Communications and Information Networks*, vol. 2, no. 4, pp. 1-10, Dec. 2017, doi: 10.1007/s41650-017-0038-2.

[18] V. Kishore, V. S. Prasad and V. V. Mani, "A Blind Timing Synchronization Algorithm for DCO-OFDM VLC Systems," *IEEE Photonics Technology Letters*, vol. 32, no. 17, pp. 1121-1124, Sept. 2020, doi: 10.1109/LPT.2020.3013447.

[19] S. Dimitrov and H. Haas, *Principles of LED Light Communications: Towards Networked Li-Fi*. Cambridge, U.K: Cambridge Univ. Press, 2015.

[20] J. Armstrong and A. J. Lowery, "Power efficient optical OFDM", *Electron. Lett.*, vol. 42, no. 6, pp. 370-372, Mar. 2006, doi:10.1049/el:20063636.

[21] S. C. J. Lee, S. Randel, F. Breyer and A. M. J. Koonen, "PAM-DMT for Intensity-Modulated and Direct-Detection Optical Communication Systems," *IEEE Photonics Technology Letters*, vol. 21, no. 23, pp. 1749-1751, Dec.2009, doi: 10.1109/LPT.2009.2032663.

[22] D. Tsonev, S. Sinanović and H. Haas, "Pulse shaping in unipolar OFDM-based modulation schemes," in *IEEE Globecom Workshops*, Anaheim, CA, USA, 2012, pp. 1208-1212, doi: 10.1109/GLOCOMW.2012.6477752.

[23] H. G. Myung, J. Lim and D. J. Goodman, "Peak-To-Average Power Ratio of Single Carrier FDMA Signals with Pulse Shaping," in *IEEE 17th International Symposium on Personal, Indoor and Mobile Radio Communications*, Helsinki, Finland, 2006, pp. 1-5, doi: 10.1109/PIMRC.2006.254407.

[24] J. Zyren, "White paper: Overview of the 3GPP long term evolution physical layer" in Austin, USA: White Paper 7, pp. 2–22, Freescale Semiconductor, Sep. 2007, [online] Available: https://www.nxp.com/docs/en/whitepaper/3GPPEVOLUTIONWP.pdf.

[25] J. Kim and H. Ryu, "Adaptive modulation for maximum throughput of multi-user SC-FDMA system in doubly selective channel," 2010 IEEE Radio and Wireless Symposium (RWS), 2010, pp. 681-684, doi: 10.1109/RWS.2010.5434143.

[26] Jing Yuan, Yan Du, Liang Gong and Jianfei Li, "A bit-loading algorithm in SC-FDE system," 2006 IEEE Radio and Wireless Symposium, 2006, pp. 27-30, doi: 10.1109/RWS.2006.1615086.

[27] Ahmad, Ayaz. "Resource Allocation and Adaptive Modulation in Uplink SC-FDMA Systems." Wireless Personal Communications 75 (2014): 2217-2242.

[28] M. Al-Rawi, R. Jantti, J. Torsner and M. Sagfors, "Opportunistic Uplilnk Scheduling for 3G LTE Systems," 2007 Innovations in Information Technologies (IIT), 2007, pp. 705-709, doi: 10.1109/IIT.2007.4430425.

[29] K. Acolatse, Y. Bar-Ness and S. K. Wilson, "Novel techniques of single-carrier frequency-domain equalization for optical wireless communications", *EURASIP Journal on Advances in Signal Process*, pp. 1-13, 2011, doi.org/10.1155/2011/393768.

[30] R Mesleh, et al. "LED nonlinearity mitigation techniques in optical wireless OFDM communication systems." *Journal of Optical Communications and Networking*, vol. 4, no. 11, pp. 865-875, 2012, doi: 10.1364/JOCN.4.000865.

[31] O. Saied, et al. "Unipolar-pulse amplitude modulation frequency division multiplexing for visible light communication systems." *Optical Engineering*, vol. 59, no. 9, pp. 096108, 2020, doi.org/10.1117/1.OE.59.9.096108.

[32] C. Wu, H. Zhang and W. Xu, "On visible light communication using LED array with DFT-Spread OFDM," in *IEEE International Conference on Communications (ICC)*, Sydney, NSW, Australia, 2014, pp. 3325-3330, doi: 10.1109/ICC.2014.6883834.

[33] O. Saied *et al*., "Single carrier optical FDM in visible light communication," in *10th International Symposium on Communication Systems, Networks and Digital Signal Processing (CSNDSP)*, Prague, Czech Republic, 2016, pp. 1-5, doi: 10.1109/CSNDSP.2016.7573947.

[34] Azim, Ali W., Yannis Le Guennec, and Ghislaine Maury. "Hermitian symmetry free optical-single-carrier frequency division multiple access for visible light communication." *Optics Communications*, vol. 415, pp. 177-185, 2018, doi.org/10.1016/j.optcom.2018.01.036.

[35] O. Saied, Z. Ghassemlooy, S. Rajbhandari and A. Burton, "Optical single carrier-interleaved frequency division multiplexing for visible light communication systems", *Optik*, vol. 194, pp. 1-7, 2019, doi.org/10.1016/j.ijleo.2019.06.010.

[36] THORLABS. PDA36A-EC - Si Switchable Gain Detector, 350-1100 nm, 10 MHz BW,13 mm2, M4 Taps, 2006, [online] Available: https://www.thorlabs.com/catalogpages/obsolete/2018/PDA36AEC.pdf.

[37] T. Zhang, H. Ji, Z. Ghassemlooy, X. Tang, B. Lin and S. Qiao, "Spectrum-Efficient Triple-Layer Hybrid Optical OFDM for IM/DD-Based Optical Wireless Communications," *IEEE Access*, vol. 8, pp. 10352-10362, 2020, doi: 10.1109/ACCESS.2020.2964792.

[38] J. G. Doblado, A. C. O. Oria, V. Baena-Lecuyer, P. Lopez and D. Perez-Calderon, "Cubic Metric Reduction for DCO-OFDM Visible Light Communication Systems," *Journal of Lightwave Technology*, vol. 33, no. 10, pp. 1971-1978, 15 May15, 2015, doi: 10.1109/JLT.2015.2402755.

[39] X. Liu, F. Effenberger, N. Chand, Lei Zhou and Huafeng Lin, "Demonstration of bandwidth-efficient mobile fronthaul enabling seamless aggregation of 36 E-UTRA-like wireless signals in a single 1.1-GHz wavelength channel," in *Optical Fiber Communications Conference and Exhibition (OFC)*, Los Angeles, CA, USA ,2015, pp. 1-3.

[40] H. B. Li et al., "Improving performance of mobile fronthaul architecture employing high order delta-sigma modulator with PAM-4 format", *Opt. Express*, vol. 25, no. 1, pp. 1-9, 2017, doi.org/10.1364/OE.25.000001.
[41] S. Yao and X. Zhang, "Joint Beamforming and DC Bias Optimization in VLC with Dimming Control," in *IEEE 85th Vehicular Technology Conference (VTC Spring)*, 2017, pp. 1-5, doi: 10.1109/VTCSpring.2017.8108581.
[42] R. C. Kizilirmak and Yau Hee Kho, "On the brightness control of ACO-OFDM based VLC systems," in *9th International Conference on Sensing Technology (ICST)*, 2015, pp. 215-218, doi: 10.1109/ICSensT.2015.7438395.
[43] S. C. Yang, *OFDMA System Analysis and Design*, MA, Norwood: Artech House, 2010.
[44] J. J. van de Beek, M. Sandell and P. O. Borjesson, "ML estimation of time and frequency offset in OFDM systems," in *IEEE Transactions on Signal Processing*, vol. 45, no. 7, pp. 1800-1805, 1997, doi: 10.1109/78.599949.
[45] J. M. Kahn and J. R. Barry, "Wireless infrared communications," *in Proceedings of the IEEE*, vol. 85, no. 2, pp. 265-298, 1997, doi: 10.1109/5.554222.

OSAMA SAIED received his higher diploma (Hons.) degree in electronic engineering from the High Institute for Poly Technics, Gharyan, Libya, in 2000. He worked as a networking engineer in Biruni Remote Sensing Center Tripoli, Libya, from 2001. He received his MSc degree in communication and signal processing from the University of Newcastle upon Tyne, United Kingdom, in 2010. He received his PhD in visible light communications from Northumbria University, Newcastle upon Tyne, United Kingdom, in 2018. He has published five journal papers and one conference paper. His research interests include optical wireless communications, free-space optics, visible light communications, and RF over optics.

XINGWANG LI. (S'14–M'15) received the B.Sc. degree in communication engineering from Henan Polytechnic University, China, in 2007, the M.Sc. degree from the National Key Laboratory of Science and Technology on Communications, University of Electronic Science and Technology of China (UESTC), in 2010, and the Ph.D. degrees in communication and information system from the State Key Laboratory of Networking and Switching Technology, Beijing University of Posts and Telecommunications (BUPT), in 2015. From 2010 to 2012, he was an Engineer with Comba Telecom Ltd., Guangzhou, China. From 2017 to 2018, he was a Visiting Scholar with the Institute of Electronics, Communications and Information Technology (ECIT), Queen's University Belfast (QUB), Belfast, U.K. He is currently an Associated Professor with the School of Physics and Electronic Information Engineering, Henan Polytechnic University, Jiaozuo, China. He has published several papers in journal and conferences, holds several patents, and has involved in several funded research projects on the wireless communications areas. His research interests include MIMO communication, cooperative communication, hardware constrained communication, NOMA, physical layer security, UAV, FSO communications, and performance analysis of fading channels. He has served a TPC member of IEEE Globecom Workshop 18'. He serves as a TPC member of IEEE/CIC ICCC workshop 19'. He currently serves as an Associate Editor of IEEE ACCESS and an Editor of the *KSII Transactions on Internet and Information Systems*

KHALED M. RABIE (Senior Member, IEEE) received the M.Sc. and Ph.D. degrees in electrical and electronic engineering from the University of Manchester, in 2011 and 2015, respectively. He is currently a Senior Lecturer with the Department of Engineering, Manchester Metropolitan University (MMU), UK. He has worked as a part of several largescale industrial projects and has published 150+ journal and conference articles (mostly IEEE). His current research interests focus on the next-generation wireless communication systems. He serves regularly on the technical program committee (TPC) for several major IEEE conferences, such as GLOBECOM, ICC, and VTC. He has received many awards over the past few years in recognition of his research contributions including the Best Student Paper Award at the IEEE ISPLC, TX, USA, 2015, the MMU Outstanding Knowledge Exchange Project award of 2016, and IEEE ACCESS Editor of the month award for August 2019. He is currently serving as an Editor of IEEE COMMUNICATIONS LETTERS, an Editor of IEEE Internet of Things Magazine, an Associate Editor of IEEE ACCESS, an Area Editor for Physical Communications (Elsevier), and an Executive Editor for the TRANSACTIONS ON EMERGING TELECOMMUNICATIONS TECHNOLOGIES (Wiley). He guest-edited many special issues in journals including IEEE Wireless Communications Magazine (2021), Electronics (2021), Sensors (2020), IEEE Access (2019). Khaled is also a Fellow of the U.K. Higher Education Academy (FHEA).